Study on Properties of Multipole Switched Reluctance Motor Designed for Multichannel Operation – Single Channel Operation Analysis

Mariusz Korkosz [1*], Piotr Bogusz[1], Jan Prokop[1], Piotr Zasowski[1]

[1] The Faculty of Electrical and Computer Engineering, Rzeszow University of Technology, Rzeszow, Poland

Abstract. The following paper deals with the multipole design of the switched reluctance motor (SRM). The design is intended to facilitate the four-channel operation of the motor. Due to multipole design of the rotor and multichannel operation abilities, there are numerous possible configurations for powering the poles in each phase. Analysis of selected such configurations was carried out, including multichannel (MC) operating conditions (e.g. single-channel operation (SCO)). A mathematical model of three-phase MC SRM is presented. The static electromagnetic torque characteristics were obtained together with the self- and mutual inductance characteristics. Selected laboratory test results are presented in the paper.

Key words: Multi-Channel, Switched Reluctance Motor, Critical Drive, Increased Redundancy Drive, Single-Channel Operation.

1. INTRODUCTION

Switched reluctance motors (SRM) belong to the brushless motor group [1]. They require a dedicated power electronics module to act as an electronic commutator. The relatively simple design of SRMs makes them highly resistant to damage. They perform very well under most of the possible fault conditions [1-5]. This makes them an excellent solution for drive systems with high redundancy requirements, such as so-called critical drives. The highest priority for a critical drive is to be able to continue operating after a critical failure. Energy efficiency is also important but less critical. Brushless motors with permanent magnets have much better operating parameters, but lack tolerance for coil shorts, for example [5]. Fault tolerance of the drive system could be improved in two ways. The first is to introduce more phases into the motor using a single power electronics system [6-10]. The second approach is based on the multichannel solution [11-14]. *N* channels are designed within a single motor, which are fed from *N* independent power electronics systems.

Both methods increase redundancy, but using a multichannel solution significantly improves the reliability of the drive system. Although this approach is more expensive to implement as it requires more power electronics systems, which take up more space, it results in improved reliability of the drive system. However, this indirectly results in some degradation of energy efficiency. The cost of implementation is justified by the improved reliability of the drive system.

An increase in the number of independent channels improves the redundancy of the drive system. Typical solutions are based on two channels. Publications on three-channel solutions are much less common. Four-channel solutions are practically non-existent in the literature.

The objective of this study is to analyse the characteristics of a Switched Reluctance Motor (SRM) designed for four-channel operation. Several power supply variants exist when considering the single-channel operation state, which differ in the length of the magnetic flux path. The study determined the characteristics of static electromagnetic torque, self-inductance, and mutual inductance for the variants considered. For the chosen motor operation point, the time courses of the phase currents and electromagnetic torque were determined. Variants in the single-channel operation range were compared to assess the asymmetry caused by mutual magnetic coupling.

2. MULTIPOLE MULTICHANNEL SWITCHED RELUCTANCE MOTOR

The design of the multipole/multichannel switched reluctance motor was suited for four-channel operation. For the quad channel (*N*=4) power supply of the three-phase (*m*=3) design, the minimum number of stator poles (N_s) is:

$$N_s = N*m*2 = 4*3*2 = 24 \qquad (1)$$

The number of rotor poles (N_r) must differ from the number of stator poles N_s by 2, eq. (2):

*e-mail: mkosz@prz.edu.pl

$$N_r = N_s \pm z * 2 \qquad (2)$$

where: $z = 1, 2 \ldots n$.

Theoretically, the following numbers of rotor poles can be employed: 22, 18, 16, etc. In practice, the motor operating point should be taken into account due to commutation frequency f_{com} 22 rotor poles would provide the highest electromagnetic torque value. At the same time, the following relation should be acknowledged:

$$f_{com} = \frac{n * N_r}{60} \qquad (3)$$

The losses in the magnetic circuit increase as the commutation frequency increases. From this point of view, a lower number of rotor poles is desirable. For the motor analysed, the minimum acceptable rotor pole number is 16.

Table I shows selected geometric parameters of the multipole, quad-channel switched reluctance motor designed by the authors.

TABLE 1. Selected geometric parameters of the SRM

Lp.	Parameter	Value
1	Numbers phases	3
2	Numbers stator poles	24
3	Numbers rotor poles	16
4	Number channel	4
5	Stator diameters	140 mm
6	Rotor diameters	82 mm
7	Shaft diameters	25 mm
8	Air-gap length	0.3 mm*
9	Active length	140 mm
10	Magnetic material	M230-35A
11	Number turn per pole	105
12	Nominal current per channel	3.5 A
13	Nominal torque per channel	2.5 N·m
14	Nominal power for SCO	375 W

*Designed

The geometry of the motor is shown in Fig. 1. The stator pole numbers used in the remainder of this paper are given in Fig. 1a. Power converter supplying the assumed channel A is shown in Fig.1b.
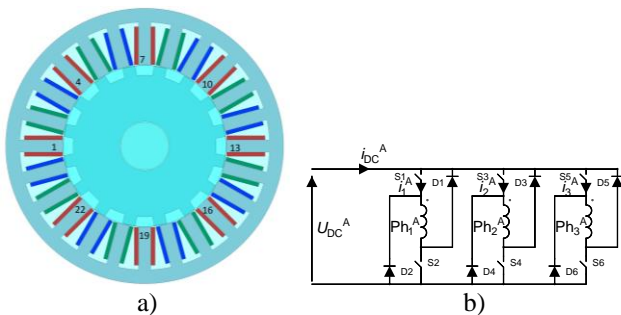
Fig.1. a) Multipole/multichannel switched reluctance motor geometry, b) Power converter for SCO SRM

3. INVESTIGATED WINDING CONFIGURATIONS

For quad-channel operation ($N=4$) and two stator poles, the total number of poles per phase is (4 x 2=8). Assuming that each channel has two N-S type stator poles (which require them to be powered accordingly), four configurations are possible. If stator poles are numbered from 1 to 24, it can be assumed that phase 1 will contain poles 1, 4, 7, 10, 13, 16, 19, 22. With this numbering, the following stator poles can form a single channel of phase 1:

1 – 4 (Case 1) – shortest magnetic flux path.
1 – 7 (Case 2) – extended magnetic flux path.
1 – 10 (Case 3) – long flux path.
1 – 13 (Case 4) – longest flux path.

The above single channel configurations differ not only in the length of the magnetic path, but also in the value of the unbalanced magnetic tension vector. Case 1 performs worst in this respect, while Case 4, with the longest magnetic path, performs best.

These configurations allow three general pole powering variants:

Variant I (*Var I*) enables pole exciting as follows: NSNSNSNSNSNS NSNSNSNSNSNS. It allows for windings configuration as in Cases 1 and 3.

Variant II (*Var II*) - stator poles are excited accordingly: NNNNNNNNNNNNSSSSSSSSSSSS. Present in Case 4 configuration.

Variant III (*Var III*) with the excitement sequence: NNSSNNSSNNSSNNSSNNSSNNSS. Suitable for Cases 1 and 2.

Single channel operation (*SCO*) is, by definition, considered a critical operating condition. It is not a prolonged operating condition. The motor should be capable of continuous operation with two channels (*DCO*). Quad-channel operation (*QCO*) goes with a reduced load on each channel. From a magnetic point of view, this corresponds to a classic motor with four branches connected in parallel. The choice of the appropriate channel configuration therefore results in the selection of one of 3 options (I, II, or III). In the case of a classic power supply (with only one channel), the choice is obvious (variant I). In the case of multi-channel operation with *SCO*, the choice is no longer so apparent.

4. MATHEMATICAL MODEL OF THE MULTICHANNEL SWITCHED RELUCTANCE MOTOR

The mathematical model of the three-phase Quad Channel Switched Reluctance Motor (*QCSRM*) in the Quad Channel Operation (*QCO*) mode is presented. The model was formulated by assuming the linearity of the magnetic circuit. The general structure of the model for phase voltage vector **u** and phase current vector **i** can be described in the following form:

$$\mathbf{u} = \mathbf{R}\,\mathbf{i} + \mathbf{L}(\theta)\frac{d}{dt}\mathbf{i} + \omega\frac{\partial \mathbf{L}(\theta)}{\partial \theta}\mathbf{i} \qquad (4)$$

$$J\frac{d\omega_m}{dt} + D\omega_m + T_L = T_e ; \qquad T_e = \frac{1}{2}\mathbf{i}^T\frac{\partial \mathbf{L}(\theta)}{\partial \theta}\mathbf{i} \quad (5)$$

2

where $T_e = T_e(\theta, \mathbf{i})$ is total electromagnetic torque. In eq. (4) - (5) vector voltage $\mathbf{u}$, vector currents $\mathbf{i}$ and matrices resistances $\mathbf{R}$, inductances $\mathbf{L}(\theta)$ are defined:

$$\mathbf{u} = \begin{bmatrix} \mathbf{u}^A \\ \mathbf{u}^B \\ \mathbf{u}^C \\ \mathbf{u}^D \end{bmatrix}; \quad \mathbf{i} = \begin{bmatrix} \mathbf{i}^A \\ \mathbf{i}^B \\ \mathbf{i}^C \\ \mathbf{i}^D \end{bmatrix}; \quad \mathbf{R} = \begin{bmatrix} \mathbf{R}^A & \mathbf{0} & \mathbf{0} & \mathbf{0} \\ \mathbf{0} & \mathbf{R}^B & \mathbf{0} & \mathbf{0} \\ \mathbf{0} & \mathbf{0} & \mathbf{R}^C & \mathbf{0} \\ \mathbf{0} & \mathbf{0} & \mathbf{0} & \mathbf{R}^D \end{bmatrix};$$

$$\mathbf{L}(\theta) = \begin{bmatrix} \mathbf{L}^{AA}(\theta) & \mathbf{L}^{AB}(\theta) & \mathbf{L}^{AC}(\theta) & \mathbf{L}^{AD}(\theta) \\ \mathbf{L}^{BA}(\theta) & \mathbf{L}^{BB}(\theta) & \mathbf{L}^{BC}(\theta) & \mathbf{L}^{BD}(\theta) \\ \mathbf{L}^{CA}(\theta) & \mathbf{L}^{CB}(\theta) & \mathbf{L}^{CC}(\theta) & \mathbf{L}^{CD}(\theta) \\ \mathbf{L}^{DA}(\theta) & \mathbf{L}^{DB}(\theta) & \mathbf{L}^{DC}(\theta) & \mathbf{L}^{DD}(\theta) \end{bmatrix} \quad (6)$$

The following symbols are used in eq. (4) - (5): θ - electrical rotor position angle, $\omega = d\theta / dt = p\,\omega_m$ - electrical angular speed, p - machine pole pairs, ω_m - the mechanical rotor speed, J - total rotor moment of inertia, D - rotor damping of viscous friction coefficient, T_L - load torque. In eq. (6) for channels $k \in (A,B,C,D)$, vectors representing phase voltages $\mathbf{u}^k$, phase currents $\mathbf{i}^k$, as well as matrices of stator resistances $\mathbf{R}^k$ and coefficients of self- and mutual inductances $\mathbf{L}^{kl}(\theta)$ are defined as follows:

$$\mathbf{u}^k = \begin{bmatrix} u_1^k, u_2^k, u_3^k \end{bmatrix}^T; \quad \mathbf{R}^k = \mathrm{diag}(R_1^k, R_2^k, R_3^k);$$

$$\mathbf{i}^k = \begin{bmatrix} i_1^k, i_2^k, i_3^k \end{bmatrix}^T; \quad \mathbf{L}^{kl}(\theta) = \begin{bmatrix} L_{11}^{kl}(\theta) & L_{12}^{kl}(\theta) & L_{13}^{kl}(\theta) \\ L_{21}^{kl}(\theta) & L_{22}^{kl}(\theta) & L_{23}^{kl}(\theta) \\ L_{31}^{kl}(\theta) & L_{32}^{kl}(\theta) & L_{33}^{kl}(\theta) \end{bmatrix} (7)$$

where for $i,j \in (1,2,3)$, $L_{ij}^{kl}(\theta)$ - coefficients of self- end mutual inductances, $k,l \in (A,B,C,D)$. The coefficients $L_{ij}^{kl}(\theta)$ depend on the rotor construction, the internal structure of the motor windings and can be expanded into a Fourier series. Finite element method (FEM) is applied on SRM mathematical model to find out the self and mutual inductances. Equations (3) - (7) generally constitute a mathematical model of the *QCSRM* in the *QCO* mode or double Dual Channel Operation (*DCO*) mode, for example, *DCO AB+CD* or *AC+BD* mode.

Similarly, equations can be written for other possible configuration cases, operating in mode *DCO* or Single Operation mode (*SCO*). For example the voltage eq. (6) and electromagnetic torque eq. (4) for the *SCO A* mode, i.e. where only channel *A* is working, can be written in the form:

$$\mathbf{u}^A = \mathbf{R}^A \mathbf{i}^A + \mathbf{L}^{AA}(\theta) \frac{d}{dt} \mathbf{i}^A + \omega \frac{\partial \mathbf{L}^{AA}(\theta)}{\partial \theta} \mathbf{i}^A \quad (8)$$

$$T_e = \frac{1}{2} \left(\mathbf{i}^A\right)^T \frac{\partial \mathbf{L}^{AA}(\theta)}{\partial \theta} \mathbf{i}^A \quad (9)$$

where vectors and matrices are defined:

$$\mathbf{u}^A = \begin{bmatrix} u_1^A, u_2^A, u_3^A \end{bmatrix}^T; \quad \mathbf{R}^A = \mathrm{diag}(R_1^A, R_2^A, R_3^A);$$

$$\mathbf{i}^A = \begin{bmatrix} i_1^A, i_2^A, i_3^A \end{bmatrix}^T;$$

$$\mathbf{L}^{AA}(\theta) = \begin{bmatrix} L_{11}^{AA}(\theta) & L_{12}^{AA}(\theta) & L_{13}^{AA}(\theta) \\ L_{21}^{AA}(\theta) & L_{22}^{AA}(\theta) & L_{23}^{AA}(\theta) \\ L_{31}^{AA}(\theta) & L_{32}^{AA}(\theta) & L_{33}^{AA}(\theta) \end{bmatrix} \quad (10)$$

Equations (8) - (9) generally constitute a mathematical model of the *QCSRM* in the *SCO* mode.
The presented *QCSRM* machine model, eq. (3) – (7), takes into account all inter-phase and inter-channel magnetic couplings. Omitting these couplings in the case of multi-channel SRM machines is unacceptable.

5. NUMERICAL TESTS RESULTS

5.1. Static characteristics of the electromagnetic torque

The numerical model was obtained in the field calculation software [15]. All configuration cases for *SCO* were investigated, including power supply variants:
- *Var I*, Case 1
- *Var III*, Case 2
- *Var I*, Case 3
- *Var II*, Case 4

In each case, the *A* channel of phase 1 was supplied with 3.5 A. The rotor position was changed within one full electrical period, i.e. 22.5 ° mech. Unaligned position of the assumed phase 1 was set as a reference position (0°).
Figure 2 shows the distribution of magnetic flux isolines for the aligned position in each of the analysed cases.

(a)

(b)

(c)

(d)
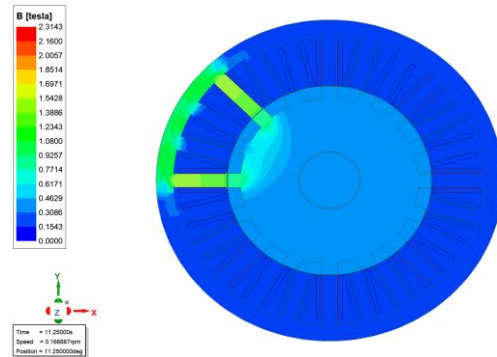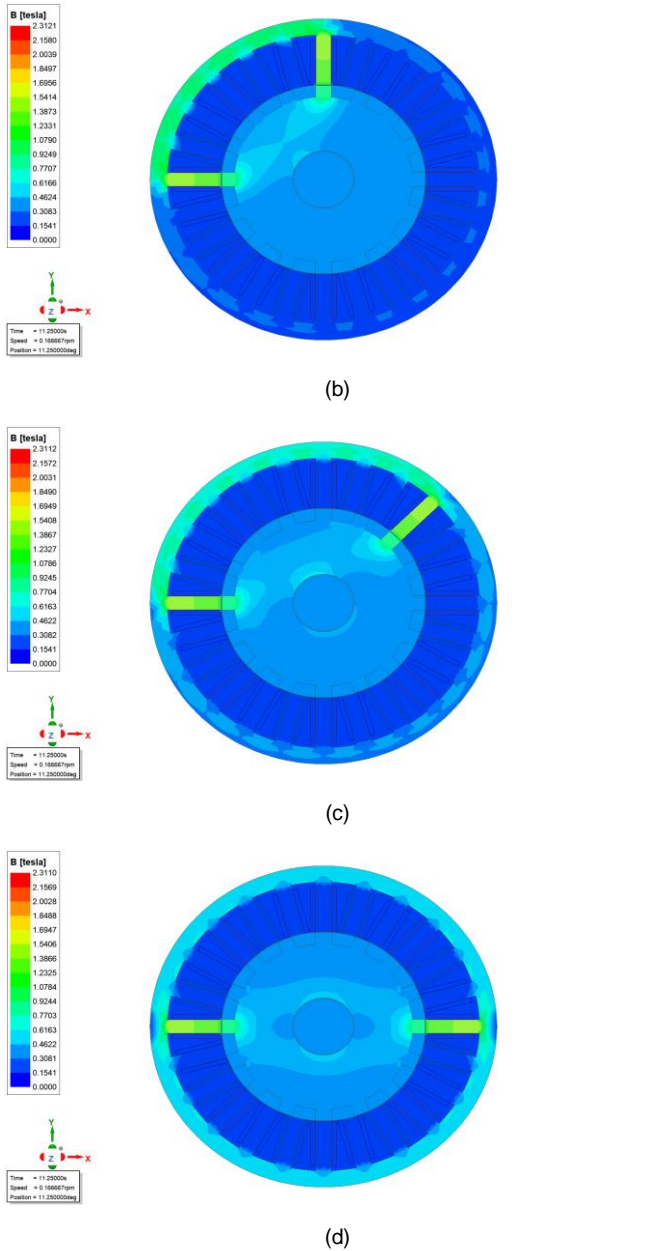
Fig.2. Isolines flux magnetics at I=3.5 A for a) Case 1, b) Case2, c) Case 3 and d) Case 4

Figure 3 shows the selected characteristics of the electromagnetic torque obtained (at I=3.5 A) as a function of the rotor position. To enhance the figure's clarity, the rotor position range was restricted to half of the electrical period.
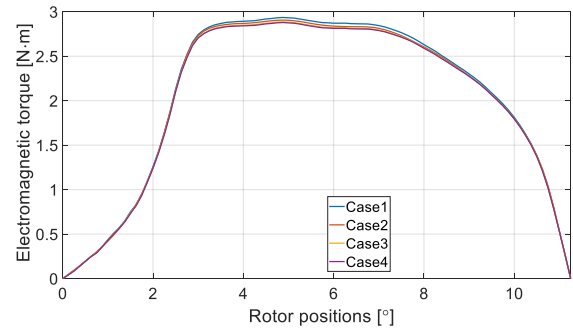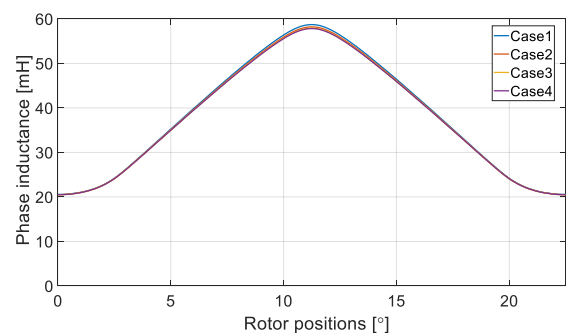

Fig.3. Electromagnetic torque vs. rotor positions at I=3.5 A for Cases 1, 2, 3 and 4

Surprisingly, in the case of single-channel operation, the electromagnetic torque value is very insensitive to the type of configuration. It is true that the electromagnetic torque produced decreases as the magnetic path length increases, but this effect is practically negligible. The main reason for this is that, in any case, it is the cross-sectional area of the stator pole and not its yoke that determines the value of the maximum induction. This can be seen in Fig. 2.

5.2. Self and mutual inductance

Self-inductance is the key parameter of the SRM. The value of the inductance of unaligned position is particularly important, as it determines the operating point of the motor. Figure 4 shows the correlation between the self-inductance of phase 1 channel A and the position of the rotor for all the cases studied.

Fig.4. Self-inductance vs. rotor positions for Cases 1, 2, 3 and 4

As with the electromagnetic torque value, very similar waveforms were obtained for each case. Although the inductance in the aligned position for case 4 is lower than for case 1, the difference is marginal.

Aligned (11.25 °) and unaligned self-inductance (0 °) in relation to phase current is shown in Figure 5.

4
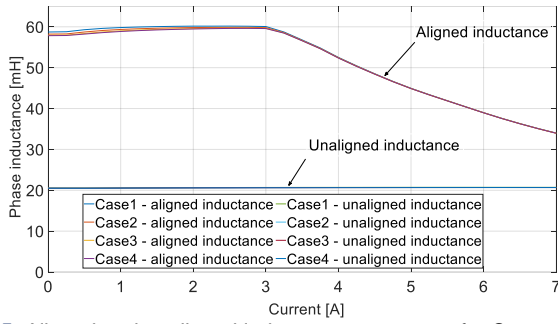
Fig.5. Aligned and unaligned inductance vs. current for Cases 1, 2, 3 and 4

Due to a large air gap (over 0.5mm), aligned self-inductance shows minimal changes in a wide current range. For currents greater than 3 A, the impact of the magnetic saturation becomes visible. Such currents are flowing mainly during overload of the single channel. Unaligned self-inductance in considered current range remains virtually constant.

In addition to the self-inductance, mutual magnetic coupling inductances are present. This concerns phase-to-phase (for one channel) and channel-to-channel coupling. The mutual coupling inductances within a channel affect the phase currents of that channel, which affects the characteristics of the electromagnetic torque. The inductances of the mutual magnetic couplings between the channels have influence in dual-channel or quad-channel operation. Figures 6-9 show the inductances of the channels' mutual magnetic couplings in the *SCO* operation for channel *A*. The mutual inductances have been determined not only within the active channel *A*, but also the conventional phase 1 with the phases of channels *B, C,* and *D*.
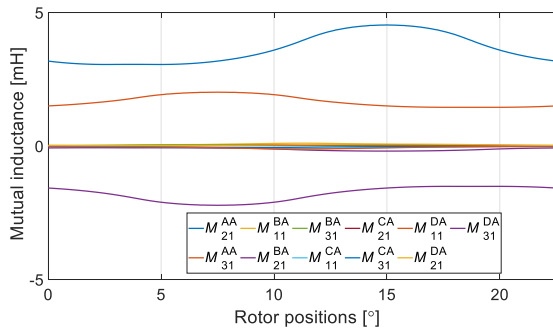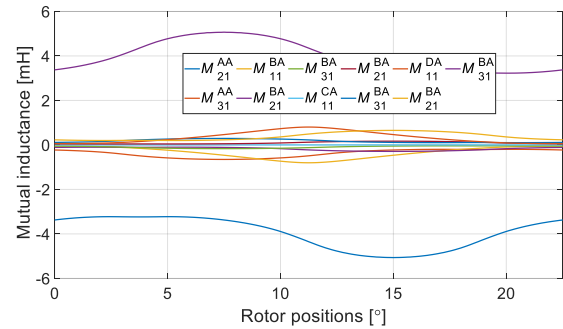

Fig.6. Mutual inductance vs. rotor positions for Case 1
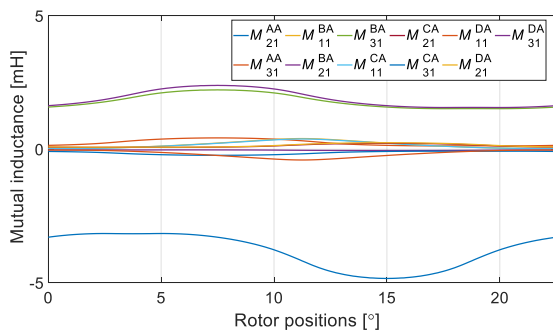
Fig.7. Mutual inductance vs. rotor positions for Case 2
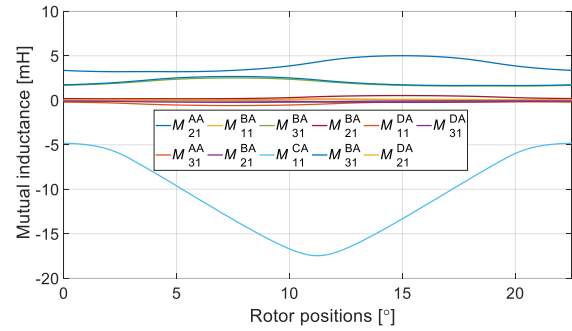
**Fig.8.** Mutual inductance vs. rotor positions for Case 3

Fig.9. Mutual inductance vs. rotor positions for Case 4

None of the analysed cases ensure complete magnetic independence between channels or within a channel. There is always at least one significant magnetic coupling within a channel or between channels.

5.3. Current and electromagnetic torque waveforms

Numerical calculations were carried out for the single-channel operation (*SCO*). The remaining motor channels were left unpowered. To show the influence of magnetic coupling, the test was carried out with single pulse control. For each case, identical control parameters were used (θ_{on}=-3.25°, θ_{off}=7.5°), and a constant speed of 1000 rpm was assumed with a 75 VDC power supply. The resulting current waveforms are shown in Fig. 10-13.
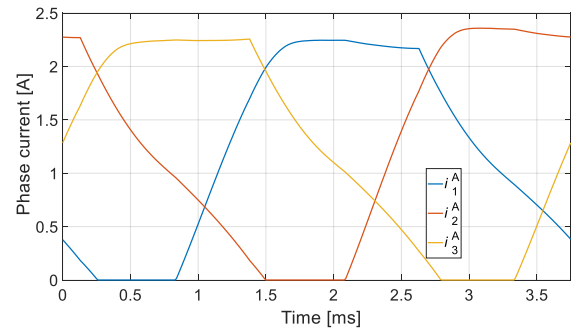
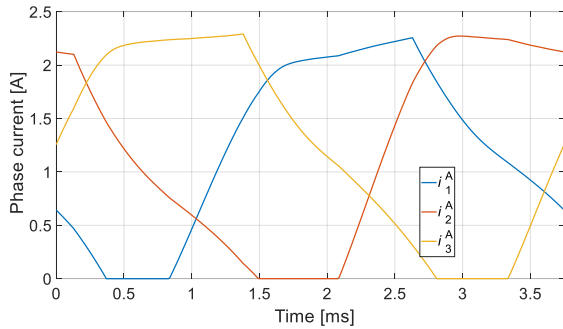**Fig.10.** Waveforms of phase currents for Case 1 – numerical test

5

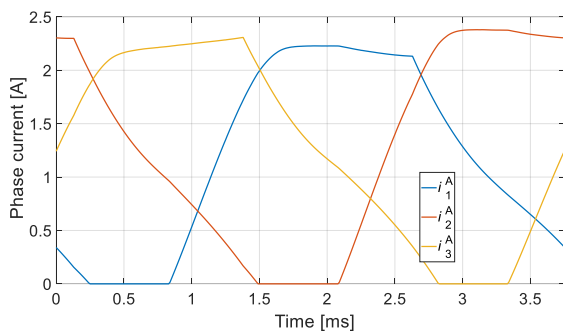**Fig.11.** Waveform of phase currents for Case 2– numerical test

Fig.12. Waveforms of phase currents for Case 3 – numerical test
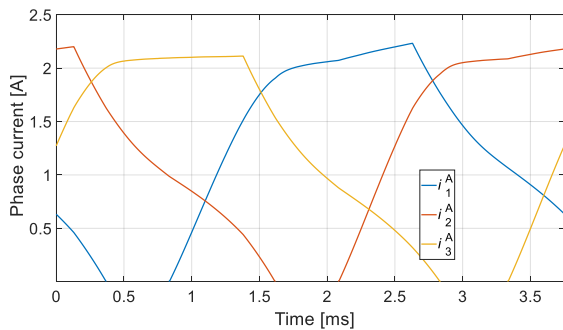

Fig.13. Waveforms of phase currents for Case 4 – numerical test

Although the characteristics of the generated electromagnetic torque (Fig.3) or self-inductance (Fig.4) are virtually identical, the resulting current waveforms for *SCO* operation are different. Current waveforms are influenced by mutual magnetic coupling. The differences can be seen in Fig. 6-7. This affects the waveform of the generated electromagnetic torque (Fig. 14).
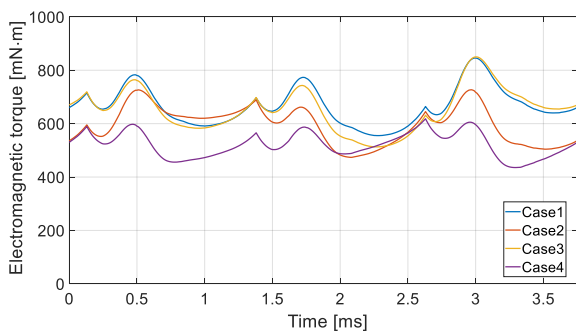

Fig.14. Waveforms of electromagnetic torque for Cases 1, 2, 3 and 4 – numerical test

The highest electromagnetic torque value is observed for case 1, lowest for case 4.

6. SELECTED LABORATORY TESTS

6.1. Electromagnetic torque

The static electromagnetic torque characteristics were determined for all cases. The laboratory test stand for the measurements of static characteristics of the electromagnetic torque is shown in Fig. 15. Tests performed under laboratory conditions yielded a family of characteristics, recorded for different values of current *I*.
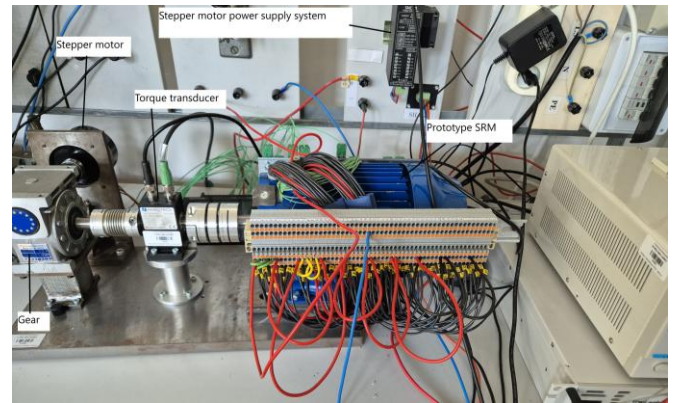

Fig.15. SRM test stand – static characteristics

The selected relationships between electromagnetic torque and rotor position are illustrated in Fig. 16. The mean value of the electromagnetic torque (T_{eav}) as a function of the current value (*I*) is shown in Fig. 17.

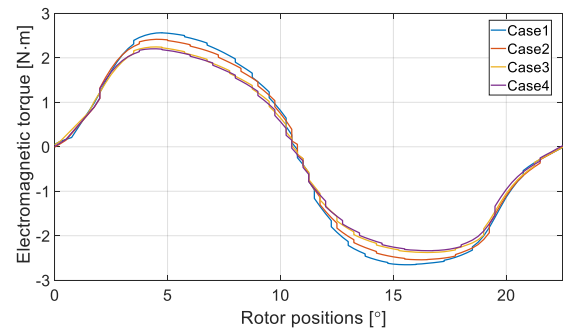**Fig.16.** Electromagnetic torque vs. rotor position for *I*=3.5A for all analysed cases
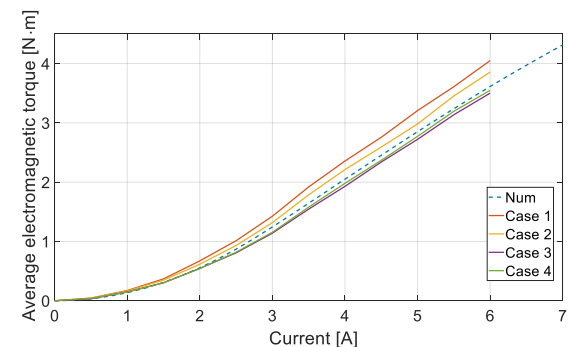

Fig.17. Average electromagnetic torque vs. current for all analysed cases

6

Although the characteristics of the generated electromagnetic torque (Fig.3) or self-inductance (Fig.4) are virtually identical, during the laboratory tests a notable disparity was observed in the torque values obtained for SCO A across the individual cases. The highest value of torque was produced by Case 1, while the lowest value was produced by Case 4. This is clearly evident in Fig. 16 for I=3.5 A. This is corroborated by the mean values obtained for the electromagnetic torque as a function of the current (Fig. 17). Fig. 17 additionally presents the results of the numerical calculations for Case 4. The discrepancy can be attributed to the fact that the results are presented for a single electrical period. In the laboratory tests, the static eccentricity of the rotor became evident. It can be observed that Cases 1 and 2 are particularly susceptible to the influence of rotor eccentricity. In contrast, Case 3 and 4 demonstrate a notable degree of immunity in this regard, attributable to the configuration of the poles (Fig. 1).

6.2. Current and electromagnetic torque waveforms

Laboratory tests were limited to determining the waveforms for the SCO operation in all cases. Figure 18 shows the test stand.
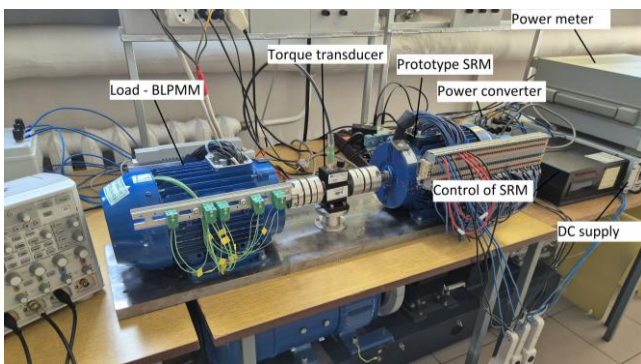

Fig.18. SRM test stand - waveforms

Laboratory tests were performed under conditions similar to numerical tests (75 VDC, 1000 rpm, (θ_{on}=-3.25°, θ_{off}=7.5°). Figures 19-22 show the recorded current waveforms for SCO operation.
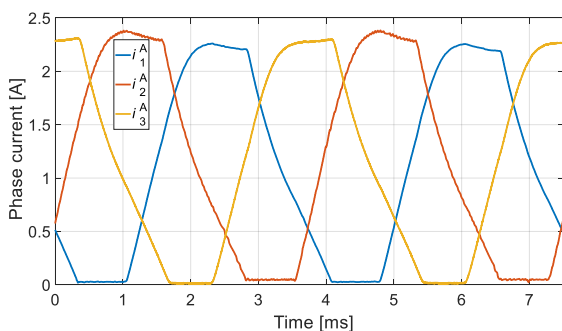

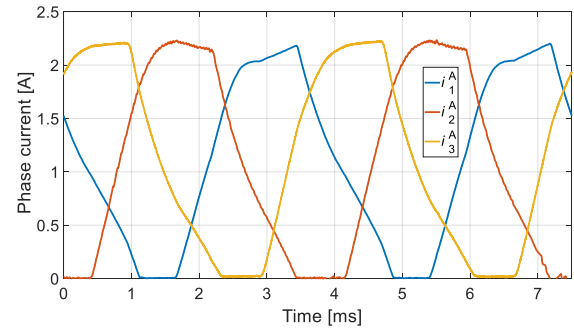**Fig.19.** Waveforms of phase currents for Case 1- laboratory test

Fig.20. Waveforms of phase currents for Case 2- laboratory test
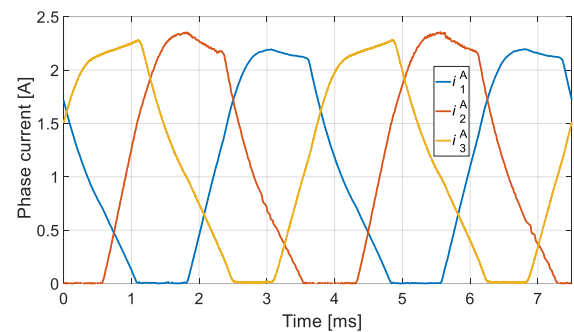
Fig.21. Waveforms of phase currents for Case 3 - laboratory test
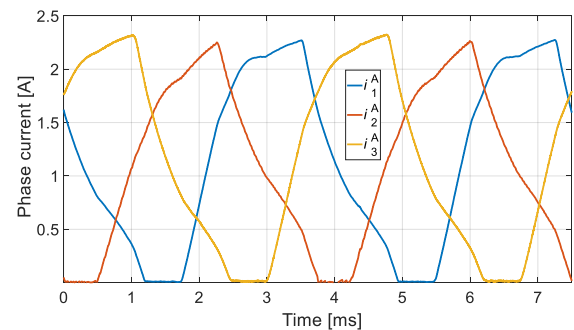
Fig.22. Waveforms of phase currents for Case 4- laboratory test

The current waveforms obtained for the *SCO* confirm the results of the numerical tests. Additionally, it is evident that the influence of magnetic couplings is greater than anticipated.

For all four cases, general efficiency of the drive system was obtained, and compared to numerical results (Table 2). For the laboratory tests, direct method was used for efficiency calculations (Eq. 11). In the numerical tests, mechanical, core and windings loses were accounted for. Loses in the converter were included in simplified manner (commutation loses were omitted)

$$\eta = \frac{P_{out}}{P_{in}} \cdot 100\% \qquad (11)$$

where: P_{out} – output power, P_{in} – input power.

TABLE 2. Overall efficiency for each analysed case

	Case 1	Case 2	Case 3	Case 4
Efficiency, [%] – numerical test	52.8	50.4	51.8	48.5
Efficiency, [%] – laboratory test	50.8	48.3	50	48.2

The highest efficiency was observed for Case 1, and the lowest for Case 4. Efficiency of a real-life system is lower than for the numerical model. This is mainly due to the lack of consideration of windings temperature increase in the model. Even though slightly higher values of the produced static electromagnetic torque are observed for Case 2 (Fig.3, Fig.16, Fig.17), Case 3 turned out to be more efficient in the numerical and laboratory tests as well. It could be explained in no other way than with the influence of interphase couplings.

6.3. Vibration velocity

The RMS value of the vibration velocity was determined during the registration of the motor current waveforms. Vibrations were measured at the drive-side bearing disc. A portable vibration analyser, the VIBSCANER, produced by Proftechnik, was employed for this purpose. Table 3 presents the RMS values of the vibration velocity obtained for the analysed *SCO* cases.

TABLE 3. Vibration velocity RMS for each analysed case

	Case 1	Case 2	Case 3	Case 4
v_{RMS}, mm/s	0.57	0.53	0.5	0.42

The results of the vibration measurement clearly indicate that Case 1 generates the highest unbalanced magnetic tension force. This results in an increase in the velocity of the motor's vibration. This is also the consequence of Case 4. The balanced magnetic tension force is observed to generate the smallest vibration.

The RMS value of the vibration velocity is a key indicator for assessing the condition of the motor. For smaller motors, a vibration velocity of less than 0.71 mm/s (RMS value) is indicative of an excellent technical condition. Nevertheless, it can be beneficial to evaluate the higher harmonic components of the vibration signal on occasion. It was possible to utilise the portable vibration analyser to achieve this. Table 3 illustrates the amplitudes of selected harmonics of the recorded vibration velocity signal.

TABLE 3. Higher vibration harmonics for each analysed case

	Case 1, mm/s	Case 2, mm/s	Case 3, mm/s	Case 4, mm/s
1st	0.45	0.43	0.4	0.37
2nd	0.06	0,05	0.05	0.04
16th	0.27	0.24	0.12	0.02

An examination of the content of the higher harmonics indicates that - typically - the first harmonic has the highest amplitude.

The relatively low value of the second harmonic of the vibration velocity is indicative of an optimal balance and alignment of the test assembly. It is noteworthy that a relatively large value of the 16th harmonic emerges. This serves as a direct confirmation of the effect of the appearance of an unbalanced magnetic tension force on the rotor. The value of the 16th harmonic is in accordance with the fundamental commutation frequency of the motor windings (eq. 3). The considerable magnitude of the unbalanced magnetic tension force is reflected in the relatively high value of the 16th harmonic of the vibration velocity. In Case 4, the amplitude of the 16th harmonic is more marginal than in the preceding cases.

Laboratory tests confirmed that Case 1 generated the highest value of electromagnetic torque (Fig16, Fig.17), while Case 4 (Table 3) produced the smallest amplitude of vibrations, as expected.

7. CONCLUSIONS

Selecting the appropriate single-channel configuration for a four-channel SRM design can be challenging. The analysis indicates that each case has implications for both two-channel and four-channel operation. Case 1, which has the shortest magnetic flux path, produces a higher torque but also results in a high value of the unbalanced magnetic tension force. Only with this configuration is it possible to achieve variant I, which provides the smallest values of phase-to-phase magnetic couplings. As a result, the phase currents of each channel will be identical, which will benefit motor operation. The Case 4 configuration, with the longest magnetic path, offers the smallest electromagnetic torque for SCO operation, but provides balanced magnetic tension, resulting in limited motor vibration. However, when multiple channels are in operation, there may be a noticeable impact of phase-to-phase and channel-to-channel magnetic couplings, resulting in undesirable effects on the phase currents. The authors suggest that the choice of channel configuration should be based on the acceptable level of machine vibration during emergency operation. If higher vibration levels are acceptable, a Case 1 configuration may be used. However, if maximum vibration reduction is required, a Case 4 configuration should be selected. Conducted test (laboratory and numerical) for SCO also point out that Case 1 provides the highest efficiency of the drive, while Case 4 efficiency is the lowest. Cases 2 and 3 are the intermediate variants. It is worth noting that although Case 3 presents slightly lower efficiency than Case 1, its' vibration level is relatively lower. It must be acknowledged that SCO is the state of operation during critical fault of the remaining channels (fault in the channels' windings or corresponding power sources).

REFERENCES

[1] T.J.E. Miller, "Switched reluctance motor and their control", *Magna Physics*, 1993.

[2] A.A. Arkadan, B.W. Kielgas, "Switched reluctance motor drive systems dynamic performance prediction under internal and external fault conditions", *IEEE Transactions on Energy Conversion*, vol. 9, no. 1, 1994, DOI: 10.1109/60.282475

[3] H. Chen, G. Han, W. Yan, S. Lu, Z. Chen, "Modeling of a Switched Reluctance Motor Under Stator Winding Fault Condition", *IEEE Transactions on Applied Superconductivity*, vol. 26, no. 4, 2016, DOI: 10.1109/TASC.2016.2539678

[4] Y. Hu, C. Gan, W. Cao, J. Zhang, W. Li, S. J. Finney, "Flexible Fault-Tolerant Topology for Switched Reluctance Motor Drives", *IEEE Transactions on Power Electronics*, vol. 31., no. 6., 2016, DOI: 10.1109/TPEL.2015.2477165

[5] M. Korkosz, P. Bogusz, J. Prokop, B. Pakla, G. Podskarbi, "Comparative Analysis of Fault-Tolerant Dual-Channel BLDC and SR Motors", *Energies*, vol. 12. No. 13, 2019, DOI: 10.3390/en12132489

[6] S. M. H. Mousavi, S. M. Mirbagheri, S.S.S.G. Sefid, S. E. S. G. Sefid, "Simulation of a new multiphase BLDC motor drive", *2012 IEEE International Conference on Power Electronics, Drives and Energy Systems (PEDES)*, DOI: 10.1109/PEDES.2012.6484304

[7] A. Mohammadpour, L. Parsa, "Global Fault-Tolerant Control Technique for Multiphase Permanent-Magnet Machines", *IEEE Transactions on Industry Applications*, vol. 51, no. 1, 2015, DOI: 10.1109/TIA.2014.2326084

[8] B. Anvari, Y. Li, H. A. Toliyat, "Design of multiphase exterior rotor switched reluctance motor for traction applications", *2016 IEEE 25th International Symposium on Industrial Electronics (ISIE)*, 2016, DOI: 10.1109/ISIE.2016.7744883

[9] B. Tian, G. Mirzaeva, Q.-T. An, L. Sun, D. Semenov, "Fault-Tolerant Control of a Five-Phase Permanent Magnet Synchronous Motor for Industry Applications", *IEEE Transactions on Industry Applications*, vol. 54., no.4, 2018, DOI: 10.1109/TIA.2018.2820060

[10] X. Deng, B. Mecrow, "A comparison of conventional and segmental rotor 12/10 switched reluctance motors", *2019 IEEE International Electric Machines & Drives Conference (IEMDC)*, 2019, DOI: 10.1109/IEMDC.2019.8785221

[11] W. Ding, "Comparative Study on Dual-Channel Switched Reluctance Generator Performances Under Single- and Dual-Channel Operation Modes", *IEEE Transactions on Energy Conversion*, vol. 27, no.3, 2012, DOI: https://doi.org/10.1109/TEC.2012.2194497

[12] W. Ding, L. Liu, J. Lou, Y. Liu, "Comparative Studies on Mutually Coupled Dual-Channel Switched Reluctance Machines With Different Winding Connections", *IEEE Transactions on Magnetics*, vol. 49, no. 11, 2013, DOI: https://doi.org/10.1109/TMAG.2013.2271753

[13] P. Bogusz., M. Korkosz, J. Prokop, "Modelling and performance analysis of dual-channel switched reluctance motor", *Archives of Electrical Engineering*, vol. 64, no. 1, pp.89-105, 2015, DOI: 10.1515/aee-2015-0009

[14] Q. Chen, D. Xu, L. Xu, J. Wang, Z. Lin, X. Zhu, "Fault-Tolerant Operation of a Novel Dual-Channel Switched Reluctance Motor Using Two 3-Phase Standard Inverters", *IEEE Transactions on Applied Superconductivity*, vol. 28, no. 3, 2018, DOI: 10.1109/TASC.2018.2799838

[15] ANSYS. *Ansys Electronics Release 2024 R1*, ANSYS Inc.: Canonsburg, PA, USA, 2024.